International Journal of Power Electronics and Drive System (IJPEDS)
Vol. 5, No. 2, October 2014, pp. 153~165
ISSN: 2088-8694

Direct Torque Control of Four Switch Three Phase Inverter Fed Induction Motor Sensorless Speed Drive

M. K. Metwally
Departement of Electrical Engineering, Menoufiya University, Faculty of Engineering, Menoufiya, Egypt

Article Info

Article history:

Received Feb 18, 2014
Revised Jul 20, 2014
Accepted Aug 15, 2014

Keyword:

Adaptive flux observer
Direct torque and flux control
Four switch three phase inverter
Induction motor
Sensorless speed control
Stator resistance identification

ABSTRACT

This paper presents sensorless speed control of induction motor (IM) using four switch three phase inverter (FSTPI) with direct torque and flux control (DTFC). The proposed sensorless DTFC system consists of an adaptive observer of rotor flux to accurately estimate stator resistance and speed simultaneously, without affecting drive performances. The switching technique for DTFC of IM using FSTPI in low power application is based on the principle of similarity between FSTPI and SSTPI (six switch three phase inverter), where the αβ plan is divided into 6 sectors and the formation of the voltage space vector is done in the same way as for SSTPI by using effective (mean) vectors. This approach allows using the well-known established switching table of SSTPI for FSTPI. The simulation results indicates that the sensorless speed control of FSTPI fed IM with DTFC and adaptive observer provides accurate estimate, good trajectory tracking with different dynamics performance. The experimental results verify the effectiveness of the proposed method at different operating points.

Corresponding Author:

M. K. Metwally,
Departement of Electrical Engineering,
Menoufiya University, Faculty of Engineering,
Menoufiya, Egypt.
Email: mohkamel2007@yahoo.com

1. INTRODUCTION

In recent years significant advances have been made on the sensorless control of IM. One of the most well known methods used for control of AC drives is the Direct Torque Control (DTC). DTC of IM is known to have a simple control structure with comparable performance to that of the field-oriented control (FOC) techniques. Unlike FOC methods, DTC techniques require utilization of hysteresis band comparators instead of flux and torque controllers. To replace the coordinate transformations and pulse width modulation (PWM) signal generators of FOC, DTC uses look-up tables to select the switching procedure based on the inverter states [1].

Direct torque control (DTC) of induction motors requires an accurate knowledge of the magnitude and angular position of the controlled flux. In DTC, the flux is conventionally obtained from the stator voltage model, using the measured stator voltages and currents. This method, utilizes open loop pure integration suffering from the well known problems of integration effects in digital systems, especially at low speeds operation range.

To obtain the simple, effective performances, fast control of torque and flux; a DTFC system for FSTPI-IM has been proposed [2]. In this paper, the optimal switching look-up table is established with four basic space vectors of FSTPI and in according with four main sectors in the αβ plan. Comparison with DTFC of induction motor fed by conventional SSTPI confirm that FSTPI topology can be alternative to the conventional topology for low power low cost induction motor drives. DTFC method for SSTPI-IM has been

improved in some researches [3-10], while the torque and speed ripples are reduced. In order to reduce the speed (torque) ripple, the space vector modulation (SVM) modulator has been used as shown in [5-9].

The switching technique for DTFC-FSTPI-IM in this paper has been done by using the new approach based on the principle of similarity between FSTPI and SSTPI [5], where the αβ plan is divided into 6 sectors and the formation of the required reference voltage space vector is done in the same way as for SSTPI by using effective (mean) vectors.

In the last decade, many researches have been carried on the design of sensorless control schemes of the IM. Most methods are basically based on the Model Reference Adaptive System schemes (MRAS) [8]. The basic MRAS algorithm is very simple but its greatest drawback is the sensitivity to uncertainties in the motor parameters. Another method based on the Extended Kalman Filter (EKF) algorithm is used [12-14]. The EKF is a stochastic state observer where nonlinear equations are linearized in every sampling period. An interesting feature of the EKF is its ability to estimate simultaneously the states and the parameters of a dynamic process. This is generally useful for both the control and the diagnosis of the process. In [14] the authors used the EKF algorithm to simultaneously estimate variables and parameters of the IM in healthy case and under different IM faults. [11] used the Luenberger Observer for state estimation of IM. The Extended Luenberger Observer (ELO) is a deterministic observer which also linearizes the equations in every sampling period. There is other type of methods for state estimation that is based on the intelligent techniques [8].

The proposed sensorless DTFC for FSTPI fed IM showed a good behavior in the transient and steady states, with an excellent disturbance rejection of the load torque. Simulation and experimental results demonstrate the effectiveness of the proposed control over different operating conditions, a precise estimation in low speed regions is obtained.

2. Space Vector Analysis of FSTPI

According to the scheme in Figure 1 the switching status is represented by binary variables S_1 to S_4, which are set to "1" when the switch is closed and "0" when open. In addition the switches in one inverter branch are controlled complementary (1 on, 1 off), therefore:

$$\begin{aligned} S_1 + S_2 &= 1 \\ S_3 + S_4 &= 1 \end{aligned} \tag{1}$$

Phase to common point voltage depends on the turning off signal of the switch as in (2):

$$\begin{aligned} V_{ao} &= (2S_1 - 1)\frac{V_{dc}}{2} \\ V_{bo} &= (2S_3 - 1)\frac{V_{dc}}{2} \\ V_{co} &= 0 \end{aligned} \tag{2}$$

Combinations of switching S_1-S_4 result in 4 general space vectors $\overline{V_1} \rightarrow \overline{V_4}$ (Fig.2, Table 1), components αβ of the voltage vectors are gained from abc voltages using Clark's transformation as in (3):

$$\begin{bmatrix} V_\alpha \\ V_\beta \end{bmatrix} = \frac{2}{3}\begin{bmatrix} 1 & -\frac{1}{2} & -\frac{1}{2} \\ 0 & \frac{\sqrt{3}}{2} & -\frac{\sqrt{3}}{2} \end{bmatrix}\begin{bmatrix} V_a \\ V_b \\ V_c \end{bmatrix} \tag{3}$$

Where V_a, V_b, V_c: output voltages on the load star connection, defined by:

$$\begin{aligned} V_a &= \frac{1}{3}(2V_{ao} - V_{bo}) \\ V_b &= \frac{1}{3}(2V_{bo} - V_{ao}) \\ V_c &= -\frac{1}{3}(V_{ao} + V_{bo}) \end{aligned} \tag{4}$$

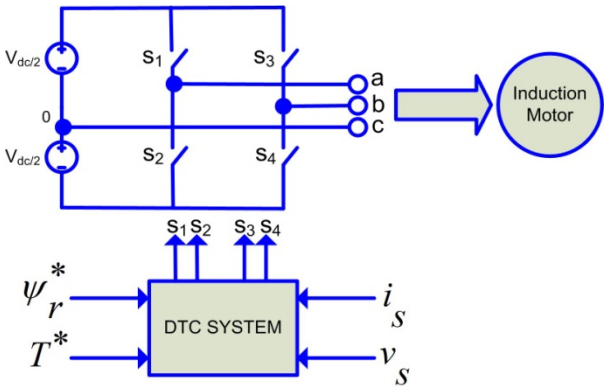

Figure 1. Power circuit of FSTPI

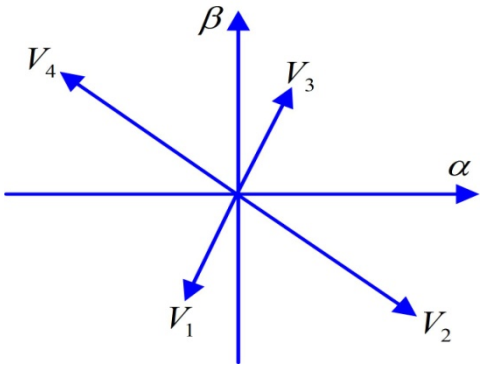

Figure 2. Voltage space vector of FSTPI in the αβ plan.

Table 1. Combination of switching and voltage space vectors

S1	S3	$\vec{V} = V_\alpha + jV_\beta$
0	0	$\vec{V}_1 = \frac{V_{dc}}{3} e^{-j\frac{2\pi}{3}}$
1	0	$\vec{V}_2 = \frac{2V_{dc}}{3} e^{-j\frac{\pi}{6}}$
1	1	$\vec{V}_3 = \frac{V_{dc}}{3} e^{j\frac{\pi}{3}}$
0	1	$\vec{V}_4 = \frac{2V_{dc}}{3} e^{j\frac{5\pi}{6}}$

To simulate six non-zero vectors in SSTPI, beside the two V_1 and V_3, it can be used the effective vectors V_{23M}, V_{43M}, V_{14M} and V_{12M}. These vectors are formed as follows:

$$\begin{aligned}
\vec{V}_{23M} &= \frac{1}{2}(\vec{V}_2 + \vec{V}_3) = \frac{V_{dc}}{3} e^{j0}; \\
\vec{V}_{43M} &= \frac{1}{2}(\vec{V}_4 + \vec{V}_3) = \frac{V_{dc}}{3} e^{j\frac{2\pi}{3}}; \\
\vec{V}_{14M} &= \frac{1}{2}(\vec{V}_1 + \vec{V}_4) = \frac{V_{dc}}{3} e^{j\pi}; \\
\vec{V}_{12M} &= \frac{1}{2}(\vec{V}_1 + \vec{V}_2) = \frac{V_{dc}}{3} e^{-j\frac{\pi}{3}};
\end{aligned} \tag{5}$$

To simulate zero vectors of SSTPI, use the effective V_{0M} as in (6):

$$\vec{V}_{0M} = \frac{1}{2}(\vec{V}_1 + \vec{V}_3) \quad (6)$$

The similarity between space vectors of FSTPI Fig.3 and SSTPI Figure 4 is presented in Table 2.

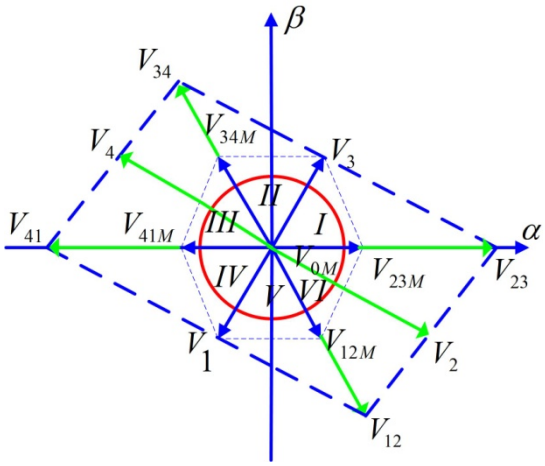

Figure 3. Voltage space vectors for (FSTPI) on the principle of similarity

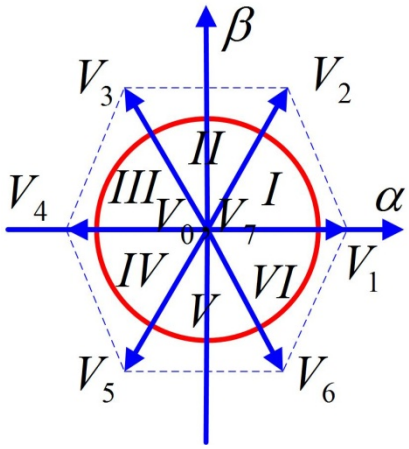

Figure 4. Base space vectors in SSTPI

Table 2. Similarity between space vectors of FSTPI and SSTPI

Used voltage space vectors for SSTPI	Used voltage space vectors for FSTPI
V1	V23M
V2	V3
V3	V43M
V4	V14M
V5	V1
V6	V12M
V0,V7	V0M

3. Modified Switching Technique for DTC

The objective of the DTC is to keep the motor torque and stator flux within a defined band of tolerance by selecting the most convenient voltage space vector from (switching table). In the case of the conventional switching table of DTC for FSTPI-IM, one of four active vectors is chosen (Table 3) [15].

Table 3. Conventional switching table for DTC control method

Δψ	ΔT	Sector1 -240^0+330^0	Sector2 30^0+60^0	Sector3 60^0+150^0	Sector4 150^0+240^0
1	1	V2	V3	V4	V1
1	-1	V1	V2	V3	V4
0	1	V3	V4	V1	V2
0	-1	V4	V1	V2	V3

In order to reduce the torque and speed ripples by using the principle of similarity for voltage space vectors, optimum switching table in the modified method is established similarly for the SSTPI switching table. The αβ plan is divided in to six sectors, and for each sector, the optimal space vector is chosen accordingly to the required torque and flux by using the effective vectors (equations 5, 6). These vectors are synthesized using the basic space vectors with the duty cycle of 50% (switching period is Ts). The same way is done for effective zero space vector (Table 4).

Table 4. Modified switching table for DTC control method

Δψ	ΔT	Sector					
		I	II	III	IV	V	VI
		-30^0 $+30^0$	30^0 $+90^0$	90^0 $+150^0$	150^0 $+210^0$	210^0 $+270^0$	270^0 $+330^0$
	1	V_3	V_{43M}	V_{14M}	V_1	V_{12M}	V_{23M}
1	-1	V_{12M}	V_{23M}	V_3	V_{43M}	V_{14M}	V_1
	0	V_{13M}	V_{13M}	V_{13M}	V_{13M}	V_{13M}	V_{13M}
	1	V_{43M}	V_{14M}	V_1	V_{12M}	V_{23M}	V_3
-1	-1	V_1	V_{12M}	V_{23M}	V_3	V_{43M}	V_{14M}
	0	V_{13M}	V_{13M}	V_{13M}	V_{13M}	V_{13M}	V_{13M}

The flux and torque calculations remain the same. The stator flux is estimated as follows:

$$\begin{aligned}\psi_{s\alpha} &= \psi_{s\alpha 0} + (v_{s\alpha} - i_{s\alpha} R_s) T_s \\ \psi_{s\beta} &= \psi_{s\beta 0} + (v_{s\beta} - i_{s\beta} R_s) T_s\end{aligned} \tag{7}$$

The estimated stator flux $\tilde{\psi}_s$ and flux angle sector are defined as follows:

$$\tilde{\psi}_s = \sqrt{\psi_{s\alpha}^2 + \psi_{s\beta}^2}\,; \theta_i = \arctan\left(\frac{\psi_{s\beta}}{\psi_{s\alpha}}\right) \tag{8}$$

The torque is estimated by the following formula:

$$\tilde{T} = \frac{3P}{2}\left(\psi_{s\alpha} i_{s\beta} - \psi_{s\beta} i_{s\alpha}\right) \tag{9}$$

Where:
- v_s, i_s Stator voltage and current vectors
- R_s Stator resistance
- P Number of pole pair
- T Electromagnetic torque
- ψ_s Stator flux vector
- T_s Sampling time

4. Rotor speed, Flux and Stator Resistance Estimation Based Adaptive Observer

To define the adaptive observer, stator voltages and currents are used to estimate the rotor flux (ψ_r), speed (ω_r), and stator resistance (R_s) according to adaptation laws that must ensure the stability of the system. Consider then the speed and resistance stator as constant parameters and unknown. The state equation of this observer is then expressed as follows by separating the state matrix in two, one for the speed and the other for stator resistance [16].

$$\dot{\hat{X}} = \left\{A_{\omega r}(\hat{\omega}_r) + A_{Rs}(\hat{R}_s)\right\}\hat{X} + BU + K(i_s - \hat{i}_s) \tag{10}$$

Where

$$A(\hat{\omega}_r) = \begin{bmatrix} a_{11} & 0 & a_2 & -a_3\hat{\omega}_r \\ 0 & a_{11} & -a_3\hat{\omega}_r & a_2 \\ a_4 & 0 & a_5 & -\hat{\omega}_r \\ 0 & a_4 & \hat{\omega}_r & a_5 \end{bmatrix}$$

and

$$A(\hat{R}_s) = \begin{bmatrix} -a_6 R_s & 0 & 0 & 0 \\ 0 & -a_6 R_s & 0 & 0 \\ 0 & 0 & 0 & 0 \\ 0 & 0 & 0 & 0 \end{bmatrix}$$

K is the observer gain matrix which governs the dynamics and the observer's robustness; it is calculated as follows:

$$K = \begin{bmatrix} K_1 & K_2 & K_3 & K_4 \\ -K_2 & K_1 & -K_4 & K_3 \end{bmatrix}^T \tag{11}$$

The coefficients K_1, K_2, $K3$, and K_4 are defined as follows:

$$K_1 = (k_1 - 1)\left(\frac{1}{\sigma L_s} + \frac{(1-\sigma)}{\sigma T_r} + \frac{1}{T_r}\right)$$

$$K_2 = (k_1 - 1)\hat{\omega}_r$$

$$K_3 = \frac{(1-k_1^2)}{a_3}\left(\frac{1}{\sigma L_s} + \frac{(1-\sigma)}{\sigma T_r} + \frac{1}{T_r}\right) + \frac{(k_1 - 1)}{a_3}\left(\frac{1}{\sigma L_s} + \frac{(1-\sigma)}{\sigma T_r} + \frac{1}{T_r}\right) \quad K_4 = \frac{(k_1 - 1)}{a_3}\hat{\omega}_r, \quad k_1 > 1$$

A hat above a symbol in (10) denotes estimated quantities, symbol T_r is the rotor time constant, L_s stator inductance, L_r rotor inductance and leakage coefficient $\sigma = 1 - L_m^2/(L_s L_r)$. The coefficient k_1 is chosen to impose a dynamic observer faster than the system. The speed adaptive mechanism can be deducted by the Lyapunov theory [17, 18].

If we choose an adequate candidate function, after application of the Lyapunov theory, the following adaptation law for the speed is gotten [17–19]:

$$\hat{\omega}_r = \left(K_{p\omega} + \frac{K_{i\omega}}{s}\right)\left(e_{is\alpha}\hat{\psi}_{r\beta} - e_{is\beta}\hat{\psi}_{r\alpha}\right) \tag{12}$$

While the stator resistance estimation is given by the adaptation law defined by:

$$\hat{R}_s = -\left(K_{pRs} + \frac{K_{iRs}}{s}\right)\left(e_{is\alpha}\hat{i}_{s\alpha} - e_{is\beta}\hat{i}_{s\beta}\right) \tag{13}$$

With $e_{is\alpha} = i_{s\alpha} - \hat{i}_{s\alpha}$ and $e_{is\beta} = i_{s\beta} - \hat{i}_{s\beta}$

Where $k_{p\omega}$, $k_{I\omega}$, k_{pRs}, k_{IRs}, are PI controller parameters of rotor speed and stator resistance adaptation mechanisms respectively.

The role of adaptive mechanisms is to minimize the following errors $\varepsilon_{\omega r}$, ε_{RS}:

$$\begin{aligned} \varepsilon_{\omega r} &= \left(e_{is\alpha}\hat{\psi}_{r\beta} - e_{is\beta}\hat{\psi}_{r\alpha}\right) \\ \varepsilon_{Rs} &= -\left(e_{is\alpha}\hat{i}_{s\alpha} - e_{is\beta}\hat{i}_{s\beta}\right) \end{aligned} \tag{14}$$

Finally, the value of speed and stator resistance can be estimated by simple PI controllers. The norm of rotor flux and its position are determined by the following relations:

$$\hat{\psi}_r = \sqrt{\hat{\psi}_{r\alpha}^2 + \hat{\psi}_{r\beta}^2} \tag{15}$$

$$\theta_r = arctg\left(\frac{\hat{\psi}_{r\alpha}}{\hat{\psi}_{r\beta}}\right) \tag{16}$$

The relation between rotor flux and stator flux as in (17)

$$\psi_r = \psi_s - i_s \sigma X_s \tag{17}$$

Where X_s is the stator reactance.

5. Drive System

The block diagram of IM DTFC drive system with proposed adaptive observer is shown in Figure 5. The system basically comprises two hysteresis controllers for flux linkage and torque control, these controllers, in conjunction with the modified switching table for FSTPI (Table 4) similarly for SSTPI switching table, generate the output signals to the gates of the power switches of the inverter.

Using the optimum switching table for FSTPI reduces the torque and speed ripples. The inverter used in this system is FSTPI.

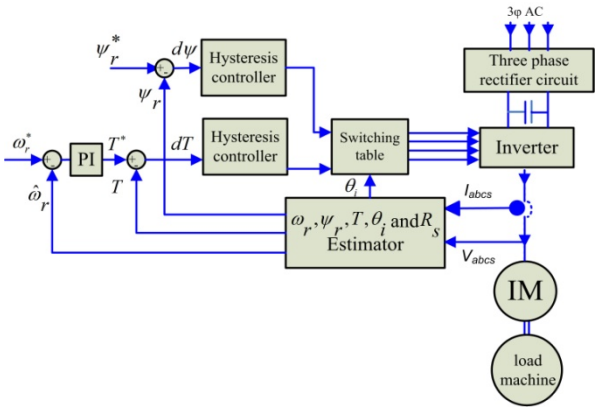

Figure 5. Block diagram of IM DTFC system

The role of the flux controller is to maintain the flux amplitude within a narrow hysteresis band around the reference value ψ_s. The torque controller receives the information obtained from the torque calculator and compares this value with the reference torque T^* (output of a speed PI controller). Two current sensors measure the motor currents (i_a, i_b) while a voltage sensor measure the motor voltages (v_a, v_b) that, in conjunction with switching table, is used to compute the stator voltages ($v_{s\alpha}$, $v_{s\beta}$). The stator flux linkage $\tilde{\psi}_s$, its angular position θ_i and estimated torque $\tilde{T}$ are given in (7), (8), (9). Also the estimated speed and stator resistance are given in (12), (13).

6. Simulation Results

Modeling and simulation work has been performed to examine the control algorithm of IM DTFC using modified switching table for FSTPI based on adaptive observer for rotor flux, speed and stator resistance estimation using MATLAB/SIMULINK software. The parameters of the induction motor prototype are listed in appendix I. The sample period T_s is 50μ_s and the load torque is set to be 5.0 N.m at 50 rpm speed and also at zero speed during forward motoring operation when the speed change to -50 rpm at t= 4sec the torque change to -5.0 N.m during reverse motoring operation.

In all simulations, the estimated speed was used for sensor-less speed control and the actual speed is presented for comparison purpose.

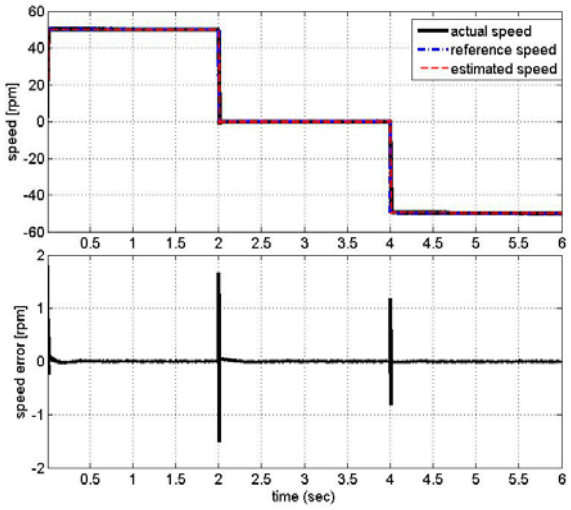

Figure 6. Upper: Reference (blue), estimated (red) and actual (black) rotor speed in rpm. Lower: speed error (rpm).

Figure 6 shows the speed waveforms under load operation when the sensorless speed control was performed using the proposed method for FSTPI the speed change from 50 rpm to zero rpm at t= 2sec with load torque equal to 6 N.m and also the speed change from zero rpm to -50 rpm at t= 4 sec as well as the load torque changes from 6 N.m to -6 N.m in the reverse motoring operation. The speed command applied in the speed controller is shown in Figure 6 upper diagram (blue) in revolution per minute (rpm) the estimated speed (red) and the actual rotor speed (black). The difference between the actual speed and estimated speed in rpm is shown in Figure 6 lower diagram. The results show the accuracy of the sensorless speed control during starting with load operation as well as speed change operations.

Figure 7 upper diagram shows a comparison between the actual rotor angle (black) and the estimated rotor angle (red) during the test depicted in Figure 6 also Fig .7 lower diagram shows the load torque (red) and the estimated torque (black) in N.m. The figures show the accuracy of the proposed technique. Figure 8 upper diagrams shows the actual rotor flux angle (black) and the estimated rotor flux angle (red), Figure 8 lower diagram shows the error between the actual and estimated rotor flux angles in degrees for the tests depicted in Figure 6. The steady state error is nearly zero which indicates that the proposed method of sensor-less speed control is very accurate with zero speed error at very low speed as well as zero speed under high load operations.

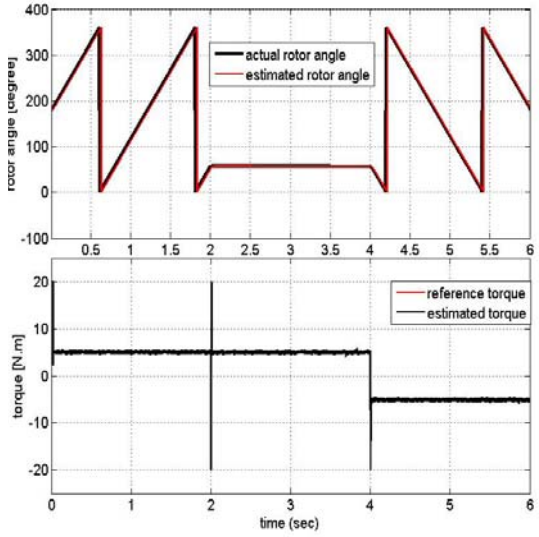

Figure 7. Upper: actual rotor angle (black), estimated rotor angle (red) in^{o}. Lower: Load torque (red) and estimated torque (black) in (N.m).

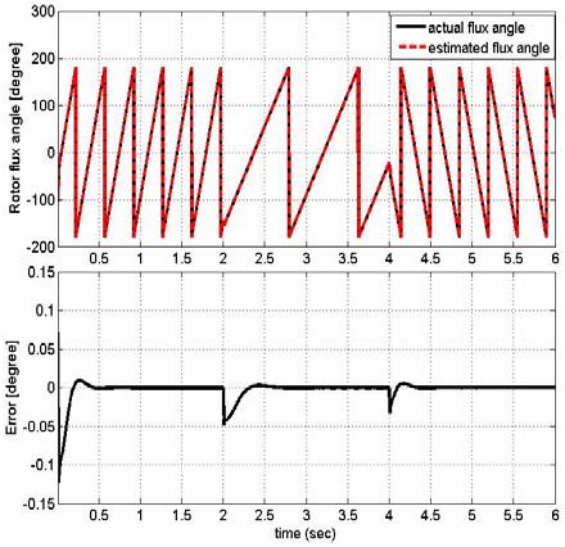

Figure 8. Upper: actual (black), estimated (red) rotor flux angle in ^{o}. Lower: Error between actual and estimated rotor flux angle in ^{o}.

Figure 9 shows the motor current in the stationary reference frame (α,β) (upper diagram) and the three phase motor currents Iabc (lower diagram).

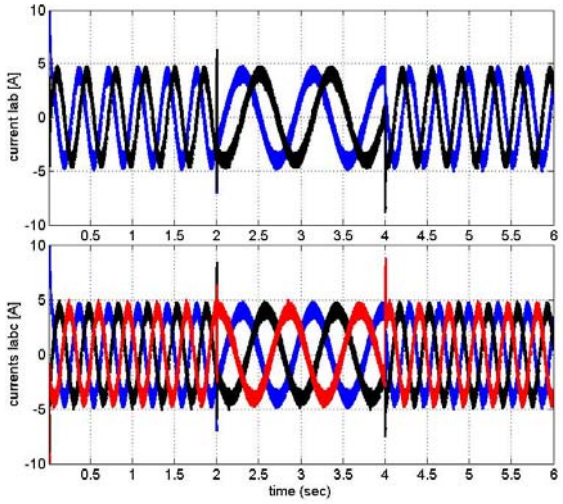

Figure 9. Upper: motor current in stationary reference frame (αβ) in (A). Lower: motor currents Iabc in (A).

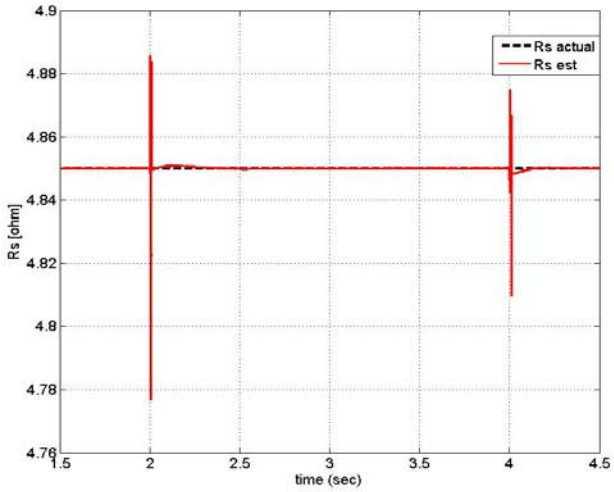

Figure 10: actual stator resistance (black-dotted) and estimated stator resistance (red) in ohm

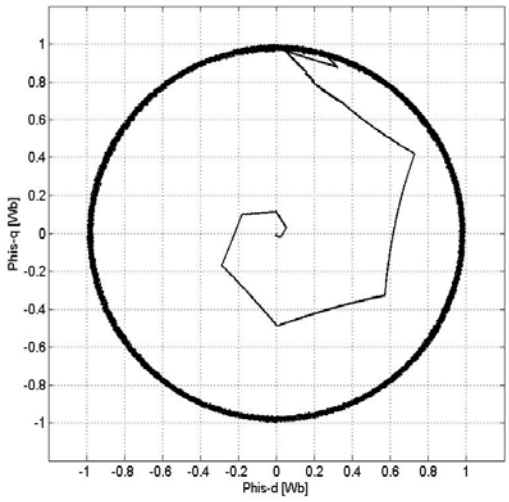

Figure 11. Stator flux linkage locus in (Wb).

Figure 10 shows the actual stator resistance and the estimated resistance using the proposed estimation algorithm during the tests depicted in Figure 6 in ohm values the figure show the accuracy of the estimation algorithm during starting with load operation. Figure 11 illustrates the stator flux linkage locus, from which it can be seen that the flux linkage vector has been running along circular locus with load operation.

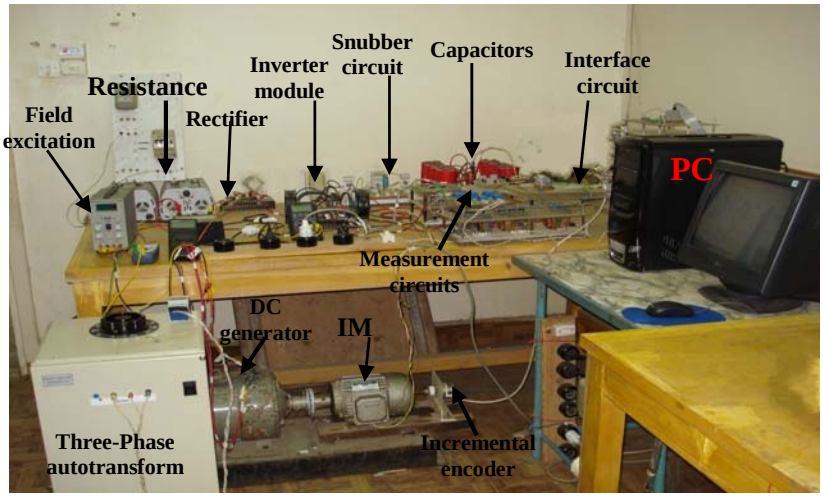

Figure 12. Experimental-setup

7. Expermental Results

The experimental results shown are from an induction machine drive coupled to a separately excited DC generator works as a load as shown in Figure 12. The machine under test was operated under sensorless speed control using DTC for FSTPI fed IM.

The torque is applied by the DC generator under torque controlled mode. The parameters of the machine under test are given in appendix. The control is done on a digital signal processor board (DSP 1103) plugged into a computer. It performs the modified DTC algorithm for FSTPI drive system fed IM.

There is a communication board for transferring and receiving data between the control algorithm on DSP 1103 and the real time system. The induction motor was fed by a voltage source inverter and two current sensors as well as two voltage sensors were used for the current and voltage measurements respectively. The proposed excitation was realized using voltage test pulses as described above. The control algorithm is executed by 'Matlab/Simulink', and downloaded to the board through host computer. The outputs of the board are logic signals, which are fed to the three phase voltage source inverter through driver and isolation circuits. The performances of the proposed DTC with speed estimation based adaptive observer with FSTPI fed IM drive under sensorless speed control are experimentally verified at different operating conditions.

The response due to a step change in the speed command is used to evaluate the performance in terms of steady state errors and stability both at no load and full load conditions. Figure 13.a shows the estimate speed response with a command speed change from 0 rpm with no load at t = 2.35 second, the speed reference has been changed to 100 rpm. It can be seen that the rotor speed is accelerated smoothly to follow its reference value with nearly zero steady state error. Figure 13.b shows the motor three phase current. The results show a good correlation between the estimated speed signal and its reference speed signals. Figure 14 shows the drive response when the motor is running with no load when speed change from 20 rpm to 40 rpm, at t=0.95 second, and then back to 20 rpm at t= 4.3 second.

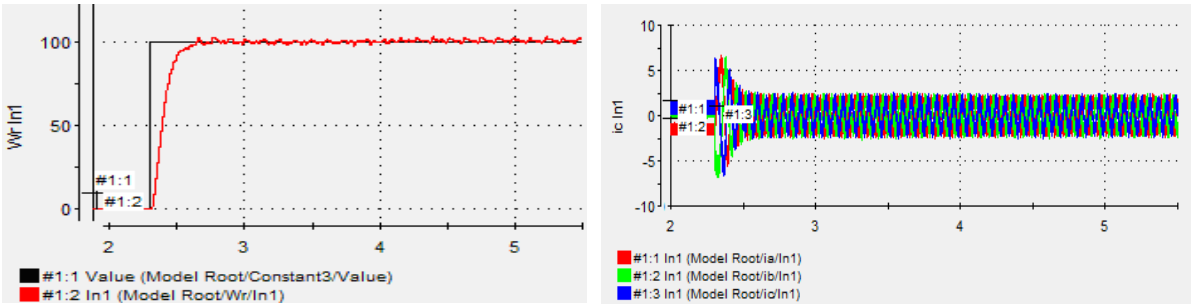

(a) (b)

Figure 13. Experimental results of FSTPI drive at no load (a) Motor Speed; (b) Three-phase motor currents.

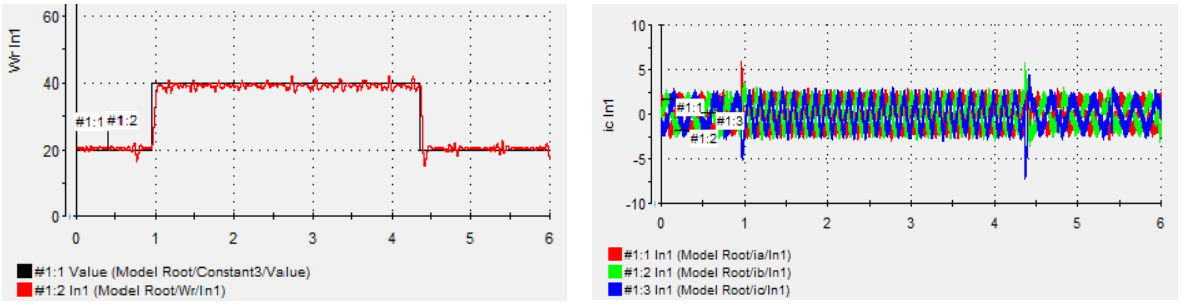

(a) (b)

Figure 14. Experimental results of FSTPI drive at no load (a) Motor Speed; (b) Three-phase motor currents.

The results shows that a perfect speed tracking with approximately zero steady state error. Figure 14.a shows that the estimated speed follows the reference speed with nearly zero steady state error. While Figure 14.b shows the motor three phase currents for the step change in speed command.

8. Conclusion

The paper presents a new approach for sensorless speed control of DTFC IM drive system using FSTPI for low power application. The modified switching table applied in this method is based on the principle of similarity between FSTPI and SSTPI, where the αβ plan is divided into 6 sectors and the formation of the voltage space vector is done in the same way as for SSTPI by using effective (mean) vectors. This approach allows using the well-knowing established switching table of SSTPI for FSTPI, in order to reduce torque ripples in comparison with the conventional DTC method for FSTPI.

The validity of new technique is verified by simulation and experimental results which demonstrate the good performance of DTC for FSTPI fed IM, while the good responses of the flux, torque, current and speed are obtained. Also adaptive flux observer used for rotor flux, speed and stator resistance estimation. The sensor-less speed control of DTFC of IM using FSTPI strategy provides fast dynamic responses with no overshoot and negligible steady-state error.

References

[1] Y Zhang., J Zhu., Z Zhao., Wei Xu., and David G. Dorrell. "An Improved Direct Torque Control for Three-Level Inverter-Fed Induction Motor Sensorless Drive", *IEEE Transactions on Power Electronics*, Vol. 27, No. 3, pp. 1502-1513, 2012.

[2] Libo Zheng, John E. Fletcher, Barry W. Williams, and Xiangning He. "A Novel Direct Torque Control Scheme for a Sensorless Five-Phase Induction Motor Drive", *IEEE Trans. on Industrial Electronics*, Vol. 58, No. 2, 2011, pp. 502-513.
[3] Aleksandar Nikolic., and Borislav Jefienic. "Speed Sensorless Direct Torque Control Implementation in a Current Source Inverter Fed Induction Motor Drive", 35th Annual IEEE Power Electronics Specialists Conference, Aachen, Germany, 2004, pp. 2843-2848.
[4] G. Foo and M. F. Rahman, "Sensorless direct torque and flux-controlled IPM synchronous motor drive at very low speed without signal injection," IEEE Trans. Ind. Electron., Vol. 57, no. 1, pp. 395–403, Jan. 2010.
[5] Bassem El Badsi, Badii Bouzidi, and Ahmed Masmoudi, "DTC Scheme for a Four-Switch Inverter-Fed Induction Motor Emulating the Six-Switch Inverter Operation" IEEE Trans. Power Electronic , Vol 28, no. 7, pp. 3528-3538, July 2013.
[6] Yen-Shin Lai, Wen-Ke Wang, and Yen-Chang Chen. "Novel switching techniques for reducing the speed ripple of AC Drives with DTC" *IEEE Trans. on Ind Electronics*, Vol. 51, No. 4, 2004, pp. 768-775.
[7] P. Q. Dzung, L. M. Phuong, and P. Q. Vinh" A new switching technique for direct torque control of induction motor using four switch three phase inverter" *in proc. IEEE PEDS* 2007, pp. 1331-1336.
[8] Cirrincione M., Pucci M., "Sensorless direct torque control of an induction motor by a TLS-based MRAS observer with adaptive integration," Automatica, 2005, 41, pp. 1843-1854.
[9] Y. Inoue, Y. Kawaguchi, S. Morimoto, and M. Sanada, "Performance improvement of sensorless IPMSM drives in a low-speed region using online parameter identification," IEEE Trans. Ind. Electron., vol. 47, no. 2, pp. 798–804, Mar./Apr. 2011.
[10] M. Hasegawa and K. Matsui, "Position sensorless control for interior permanent magnet synchronous motor using adaptive flux observer with inductance identification," IET Electr. Power Appl., vol. 3, no. 3, pp. 209–217, May 2009.
[11] Kyo B. L., Frede B., "Reduced-Order Extended Luenberger Observer Based Sensorless Vector Control Driven by Matrix Converter With Nonlinearity Compensation," IEEE *Trans. Ind. Electron*., 2006, Vol 53, pp. 66-75.
[12] Jin-Su Jang, Byoung-Gun Park, Tae-Sung Kim, Dong Myung Lee, Dong-Seok Hyun, "Sensorless Control of Four-Switch Three-Phase PMSM Drive Using Extended Kalman Filter" IEEE IECON Conference, pp.1368-1372, June 2008.
[13] Murat Barut., Seta Bogosyan., and Metin Gokasan, "Speed-Sensorless Estimation for Induction Motors Using Extended Kalman Filters", *IEEE Transactions on Industrial Electronics*, Vol. 54, No. 1, February 2007.
[14] I. M. Alsofyani, NRN Idris, T. Sutikno, and Y. A. Alamri. "An Optimized Extended Kalman Filter for Speed Sensorless Direct Troque Control of an Induction Motor", IEEE International Conference on Power and Energy, 2-5 December 2012, Kota Kinabalu Sabah, Malaysia.
[15] Mohamed Azab and A.L. Orille, "Novel Flux and Torque Control of IM Drive using FSTPI", *in IEEE Proceeding IECON conference,* 2001,pp 1268 -1273.
[16] Suwankawin S, Sangwongwanich S, "Design strategy of an adaptive full-order observer for speed-sensorless induction-motor drives-tracking performance and stabilization," *IEEE Trans. on Industrial Electronics*, vol. 53, no. 1, pp.96–119, 2006.
[17] Harnefors L, Hinkkanen M, "Complete stability of reduced-order and full-order observers for sensorless IM drives*," IEEE Trans. on Industrial Electronics* 2008; 55(3):1319–1329.
[18] Vaclavek P, Blaha P, "Lyapunov-function-based flux and speed observer for AC induction motor sensorless control and parameters estimation," *IEEE Trans. on Industrial Electronics* 2006; 53(1):138–145.
[19] Etien E, Bensiali N, Chaine C, Champenois G, "Adaptive speed observers for sensorless control of induction motor : a new criterion of stability," International Review of Electrical Engineering 2006; 1:36–43.

Appendix I. The parameters of applied induction machine

Parameter	Value
Rated power	1 kW
No. of poles	4
Stator resistance	4.85 ohm
Rotor resistance	2.6840 ohm
Rotor leakage inductance	0.0221 H
Stator leakage inductance	0.0221 H
Mutual inductance	0.4114 H
Supply frequency	50 Hz
Motor speed	1420 r.p.m.
Supply voltage	380 volts
Inertia	0.018 $kg.m^2$